109 Ag– 107 Ag fractionation in fluids with applications to ore deposits, archeometry, and cosmochemistry

Toshiyuki Fujii, Francis Albarède

Available online at www.sciencedirect.com

ScienceDirect

Geochimica et Cosmochimica Acta 234 (2018) 37–49

Geochimica et Cosmochimica Acta

www.elsevier.com/locate/gca

^{109}Ag–^{107}Ag fractionation in fluids with applications to ore deposits, archeometry, and cosmochemistry

Toshiyuki Fujii [a], Francis Albarede [b,*]

[a] Division of Sustainable Energy and Environmental Engineering, Graduate School of Engineering, Osaka University, 2-1 Yamadaoka, Suita, Osaka 565-0871, Japan

[b] Ecole Normale Supérieure and Université de Lyon, 46 allée d'Italie, 69007 Lyon, France

Received 8 January 2018; accepted in revised form 8 May 2018;

Abstract

Evidence of $^{109}Ag/^{107}Ag$ variability in ancient silver coins led us to calculate the reduced partition functions for ^{107}Ag and ^{109}Ag in various dissolved Ag species by *ab initio* methods in order to evaluate the extent of Ag fractionation in fluids and the potential of Ag isotopes to discriminate between different metal sources. We used a hybrid density functional implemented by the Gaussian 09 code and consisting of Bickley's three-parameter non-local hybrid exchange potential with Lee-Yang-Parr non-local functionals. The ratios ln β of reduced partition functions were for the free Ag^+ ion with various degrees of hydration, hydrates, chloride complexes, sulfides, sulfates, Sb-As sulfosalts, and Ag-ammines. At 0 °C, the magnitude of the nuclear field shift effect between metal and dissolved sulfide is -1×10^{-4}. Using literature stability fields at different temperatures, we conclude that only weak Ag isotope fractionation is expected in the Ag-Cl-S system regardless of the pH of hydrothermal solutions at 300 °C. Stronger effects are predicted when Sb and As are added to the solutions. Bonding with SbS_3 and AsS_3 reduces ln β values by $\sim 2 \times 10^{-4}$. Under the more oxic conditions of the subsurface and at the temperatures of groundwater, Ag should be present as Ag^+ and, at higher chlorinity, as $AgCl^0$. The latter component is isotopically heavier than Ag^+. In groundwater underneath forests and grasslands, ammonia resulting from nitrogen fixation produces the particularly strong complex known as di-ammine silver $Ag(NH_3)_2^+$ (Tollen's reagent). Upon reduction by aldehydes and melanin, $Ag(NH_3)_2^+$ precipitates metallic Ag(0). Biological oxidation of NH_3 to NO_2^- and NO_3^- (nitrification) also is expected to destroy $Ag(NH_3)_2^+$ and precipitate metallic Ag(0). Both chloragyrite (AgCl) and native Ag are found among the weathering products (gossan) of bedrock ore deposits. The high end of the $^{109}Ag/^{107}Ag$ histogram of silver coinage from around the Mediterranean and from Spanish Americas, particularly well-represented in Mexican silver ore, therefore attests to the presence of gossan silver, while the variability at the low end is more likely to represent temperature effects and variable abundances of S, Sb, and As in hydrothermal fluids. Should the yield of Ag during separation chemistry be less than 100%, or samples be altered by metamorphism, low-temperature Ag isotope fractionation becomes an issue seriously affecting (i) so-far published $^{109}Ag/^{107}Ag$ data on chondrites, (ii) ages derived from the extinct ^{107}Pd–^{107}Ag chronometer ($T_{1/2} = 6.5$ Ma), and (iii) inferences about the volatile content of the Earth. It is argued that the NIST SRM 978a value should be retained to represent the Bulk Silicate Earth and not the literature values on basalts, which clearly have been affected by incomplete Ag separation.

Keywords: Silver; Silver isotopes; Silver ores; Galena; Ab initio; Solutions; Coins

1. INTRODUCTION

For over 2700 years, silver and money have been so intimately related that in some languages they are designated

* Corresponding author.
E-mail addresses: fujii@see.eng.osaka-u.ac.jp (T. Fujii), albarede@ens-lyon.fr (F. Albarede).

https://doi.org/10.1016/j.gca.2018.05.013
0016-7037/

by the same word. Silver, which permeates societies much more pervasively than gold and is still considered precious compared to copper, propelled states such as Persia, Athens, Carthage, and Rome to the status of empires by boosting trade and allowing mercenary armies to be hired. The value of silver was first recognized by the early cultures of Mesopotamia but was used largely for plates, cutlery, statues, and religious objects. It was not until the introduction of coinage in Asia Minor during the 7th century BC that long-distance trade and war tributes were born, which represented one of the turning points in human history.

In the Mediterranean world, the rise and fall of empires coincide with the discovery and demise of major silver ore deposits. The Laurion mines established Athens as the leading city-state in the 5th century BC Greece, with the famous owl coin assuming the same global role as the modern dollar. The silver mines from Southern Iberia brought immense power to Carthage and, from the mid-3rd century BC onwards, to Rome, allowing a flourishing trade between the Roman Empire and peoples around the Indian Ocean (McLaughlin, 2014) and established the *denarius* as the major currency for almost two millennia. It is remarkable how faithfully the number of shipwrecks in the Mediterranean tracks lead contamination associated with the mining of argentiferous galena (Parker, 1992; Hong et al., 1994; Kylander et al., 2005; Scheidel, 2009). Silver from Peru (Potosi) and Mexico (Zacatecas) changed the pattern of war in Europe in the 16th and 17th c. AD (Garner, 1988) and, by fueling long-distance trade, financed China's monetization and economic expansion (Flynn and Giraldez, 1996; von Glahn, 2003; Spate, 2013). Establishing the origins of silver coins and artifacts therefore is key to understanding how past empires rose and fell through the millennia. A very brief description of some historically significant Ag ore deposits (Boyle, 1968) is given in the Appendix.

The most common hydrothermal silver-bearing mineral is galena (PbS) which can hold up to 0.4 mol percent Ag (Van Hook, 1960) mostly substituted by miargyrite-proustite $Ag(Sb,As)S_2$ (Chutas et al., 2008; Renock and Becker, 2011; George et al., 2015), argentite/acanthite (Ag_2S), and pyrargyrite (Ag_3SbS_3), or in substitution for Cu in sulfosalts from the tennantite-tetrahedrite $Cu_{12}([As, Sb]S_3)_4S$ series. Silver chloride AgCl (chlorargyrite) and native Ag form at low temperatures in gossan produced by weathering of underlying ore deposits, and more generally in soils (Boyle, 1968).

The relative abundances of Pb isotopes have been used for decades to trace the provenance of artifacts (Brill and Shields, 1972; Gentner et al., 1978; Stos-Gale and Gale, 2009). Most studies do not go beyond a simple comparison of Pb isotopic ratios between a particular artifact and ores that may have been the potential sources of its metal. If relative abundances of Pb isotopes in rocks vary, it is an expression of the ore environment, typically the tectonic age of the province hosting the ore deposits, and the long-term U/Pb and Th/U ratios of their sources (Blichert-Toft et al., 2016). Using Pb isotopes to trace the origin of Ag has, however, been criticized on the basis that Pb and Ag held in a particular silver coin may derive from different sources (Budd et al., 1996). This is unlikely in the case of Ag extracted from argentiferous galena: local ores are such an obvious source of local Pb used for Ag cupellation (purification) that import is unnecessary. Extraneity of Pb and Ag is much more likely to be the case for silver extracted from sulfosalt ores, which in general contain little lead: cupellation is therefore carried out using Pb from a different provenance. It may also be a result of reminting under duress, like at the climax of the second Punic War (Albarède et al., 2016).

The isotopic abundances of other metals involved in coinage, Au, Cu, and Ag, have so far been given relatively little attention. Gold has only one stable isotope which excludes this element from isotopic analysis, while $^{65}Cu/^{63}Cu$ shows a broad range of variation (Klein et al., 2010) due to variable speciation of Cu in fluids and variable deposition temperatures. Copper is not even systematically associated with Ag ores (Boyle, 1968) but small amounts of Cu often were added to silver coinage to improve its mechanical properties and for the purpose of debasement. In this case the risk was that adding Cu beyond eutectic proportions (28.1 wt%) (Baker and Okamoto, 1992) would render the retrieving of Ag for reminting very costly.

The relative abundances of the ^{107}Ag and ^{109}Ag isotopes are particularly appealing because silver carries all the coinage value. Athenian owls, the drachmas of Alexander and his successors, the denarii of the Roman Republic, and the 16th century pieces-of-eight (the ancestor of the dollar) are noticeable for their Ag fineness. The variability of Ag isotopic abundances in ancient coins was established by Desaulty and Albarede (2013), Desaulty et al. (2011) and Albarède et al., 2016 (Fig. 1). As expected from the heavy masses of these isotopes, their compositional range is fairly narrow: defining ε_{109Ag} as the deviation of the $^{109}Ag/^{107}Ag$ ratio measured in a given sample from that of the NIST SRM 978a standard in parts per 10,000, most silver coins fall between −1 and +2. The analytical precision of 5–10 ppm is sufficient to reveal statistically significant differences between historically and geographically different sets of coins. In contrast, native silver ores analyzed by Hauri et al. (2000), Chugaev and Chernyshev (2009), and Mathur et al. (2018) show a range in ε_{109Ag} from −5.3 to +1.9, which is much broader than that of silver coinage from around the Mediterranean and from Spanish Americas analyzed by Desaulty and Albarede (2013), Desaulty et al. (2011) and Albarède et al., 2016, arguing against native ores being used as a major source of metal. Given the growing interest in silver isotopes, understanding the causes of Ag isotopic variability therefore is a timely undertaking and what the present work aims to achieve is to provide a first compendium of *ab initio* calculations of Ag isotope fractionation between species coexisting in fluids between 0 and 300 °C. We will compute stable structures, interatomic distances, and ln β values, where β stands for reduced partition function ratios of isotopologues, and, using the work by Akinfiev and Zotov (2001) on Ag speciation in hydrothermal fluids, discuss isotope fractionation between the different ore minerals that host silver. We will show that isotope fractionation among coexisting species sheds light on the origin of isotopic variability among different Ag sources.

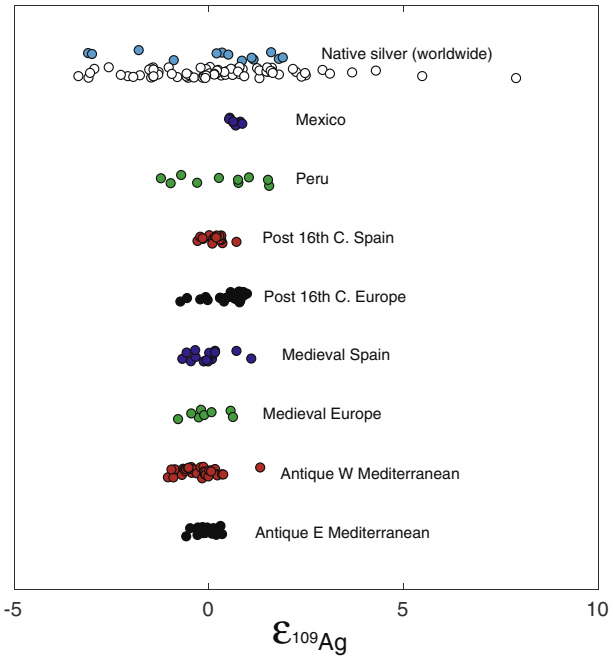

Fig. 1. Literature data reported as ε_{109Ag} (the deviation of $^{109}Ag/^{107}Ag$ of a given sample from $^{109}Ag/^{107}Ag$ of the NIST SRM 978a standard in parts per 10,000). The data upwards from the Antique East Mediterranean to Mexico represent analyses of 132 silver coins (Albarède et al., 2016; Desaulty and Albarede, 2013; Desaulty et al., 2011). Typical 2-sigma errors are 0.05–0.08 εunits. The top row represents values of native silver and silver in gold with typical 2-sigma errors of 0.2–0.4 ε units (blue: Chugaev and Chernyshev (2009); open symbols: Mathur et al. (Mathur et al., 2018)). (For interpretation of the references to colour in this figure legend, the reader is referred to the web version of this article.)

The contribution of nuclear field shift or 'nuclear volume' (Fujii et al., 2009b; Schauble, 2007) to isotopic fractionation also needs to be estimated. These terms refer to what is actually the zeroth (mean radius) and second order terms (shape) of the tensor of nuclear charge distribution, both identified by nuclear spectroscopy in the '30s. The topic has been covered multiple times, notably by Brix and Kopfermann (1958), Breit (1958), and King (1984). The nuclear field-shift (NFS) effect on stable isotope abundances received a theoretical treatment by Bigeleisen (1996). It was suggested by, respectively, (Fujii et al., 2006a, 2006b) and (Schauble, 2007) that NFS could alter the apparent amplitude of nucleosynthetic anomalies in meteorites and the natural isotopic abundances of heavy elements. For silver, which has only two stable isotopes, NFS is difficult to observe analytically and its theoretical prediction by *ab initio* techniques is therefore particularly useful.

Finally, we use our results to address one of the long-standing challenges posed by the extinct ^{107}Pd-^{107}Ag chronometer in meteorites ($T_{1/2} = 6.5$ Ma), which is to understand the rather large scatter of data on chondrites with little radiogenic ^{107}Ag. We conclude that isotope fractionation by low-temperature alteration makes this chronometer inadequate to handle the issues of element volatility in the early Solar System.

2. METHODS

Orbital geometries and vibrational frequencies of Ag species were computed using the density functional theory (DFT) implemented by the Gaussian09 code (Dennington et al., 2009; Frisch et al., 2009). The DFT method employed here is a hybrid density functional consisting of Becke's three-parameter non-local hybrid exchange potential (B3) (Becke, 1993) with Lee-Yang-and Parr (LYP) (Lee et al., 1988) non-local functionals. The 6-311+G(d,p) basis set, which is an all-electron basis set, was used for H, C, N, O, Na, S, Cl, and As. For Ag and Sb, aug-cc-pVTZ basis set (Figgen et al., 2005; Peterson and Puzzarini, 2005), which is an effective core potential (ECP) basis set, was used. Molecules were modeled without any forced symmetry. An ultrafine numerical integration grid was used and the SCF (self-consistent field) convergence criterion was set to 10^{-8}. Calculations were performed for single cluster model molecules. Short-range properties of ions and compounds with the solution are often evaluated by assuming that they are surrounded by a fixed frame of water molecules arranged to form a second solvation shell (large clusters) (Fujii et al., 2010; Rustad et al., 2010). This topic was recently reviewed by Blanchard et al. (2017). The large cluster model, however, needs experimental evidence of molecular arrangement in the second coordination sphere (Fujii et al., 2014) and also raises some difficulties for the choice of the basis set (Rustad et al., 2010). In addition, water exchange with the solution is so fast, at least in the case of solutions of silver chlorides, that the hydration shells cannot be considered as regular or stable (Liu et al., 2012). For the calculation of long range interactions, it may be assumed that the whole complex immersed in a continuum with dielectric properties approximating those of the solvent (Tomasi et al., 2005; Ginovska et al., 2008). The effect of a polarizable continuum is, however, smaller than that of a second coordination sphere (Fujii et al., 2014). For this preliminary work, we therefore restricted our calculations to a single-coordination shell (small clusters, typically $Ag(H_2O)_6^+$) with no additional water shell.

The isotope enrichment factor was evaluated from the reduced partition function ratio (RPFR) $(s/s')f$ (Bigeleisen and Mayer, 1947; Urey, 1947), also noted β, such as

$$\ln \frac{s}{s'} f = \sum [\ln b(u_i') - \ln b(u_i)] \quad (1)$$

where

$$\ln b(u_i) = -\ln u_i + \frac{u_i}{2} + \ln(1 - e^{-u_i}) \quad (2)$$

and

$$u_i = \frac{h\nu_i}{kT} \quad (3)$$

In the latter expression, ν stands for vibrational frequency, s for the symmetry number of the considered compound, h for the Plank constant, k for the Boltzmann constant, and T for the absolute temperature. The subscript i denotes the i-th normal mode of molecular vibration, and primed variables refer to the light isotopologue. The isotope enrichment factor due to molecular vibrations can be eval-

uated from the frequencies ν_i summed over all the different normal modes. In order to represent true isotope fractionation factors, the ln β values should be corrected with different terms accounting for inharmonic vibrations, for the Born-Oppenheimer approximation, for the nuclear spin effect, and for the nuclear field shift effect. Of all these corrections, only the last term is deemed significant (Bigeleisen, 1996; Fujii et al., 2009a).

The hydration number of Ag^+ ions had been thought to be two (Maeda et al., 1979). Then the tetracoordination was suggested with a 2.4 Å bonding distance of Ag—O (Sandstrom et al., 1985; Magini, 2018). In an X-ray absorption fine structure (EXAFS) and large-angle X-ray scattering (LAXS) study, a combination of two shorter Ag—O and two longer Ag—O distances was discussed (Persson and Nilsson, 2006). The data are reported in Table 1. In a molecular dynamics (MD) study (Blauth et al., 2010) and an EXAFS study (Fulton et al., 2009), pentacoordination and hexacoordination (a distorted octahedral) structures of hydrated Ag^+ were presented as well as the tetracoordination. In this study, the bonding distances calculated for the tetracoordination showed a mixture of short and long Ag—O distances. Calculation of the hexacoordination resulted in a distorted octahedral structure with two $Ag—O_{axial}$ and four $Ag—O_{equatorial}$, but the variation of the Ag—O bonding distance was only 0.05 Å. The ln β values of the hydrated Ag^+ ions are shown in Table 2. As shown in Table 2, ln β decreased with the hydration number. Hence, the accurate structure of hydrated Ag^+ ions should be experimentally clarified.

The ligands, which possess π bonding character, form strong complexes with Ag(I) and tend to form liner structures, where H_2O and OH^- are poor examples of the twofold coordination of Ag(I) (Baes and Mesmer, 1976). As for the twofold linear coordination complexes, Ag(I) hydroxide, chloride, sulfate, and sulfide, were computed. The ln β values obtained are shown in Table 2. Since SO_4^{2-} is a strong divalent anion, an initial structure of linear H_2O-Ag-SO_4 turned to bend and H_2O and SO_4^{2-} was contacted. This may have resulted in a small ln β for $AgSO_4(H_2O)$ The order of ln β for the complexation between $Ag(H_2O)^+$ and L (L: H_2O, OH^-, Cl^-, HS^-, HSO_4^-) was found to be $OH^- > Cl^- > HSO_4^- > HS^- > H_2O$. Deprotonation of hydrated Ag^+ may create a large isotope fractionation. Besides

Table 1
Values of ratios of reduced partition functions, in the form of 1000 ln β, for the isotopomers of different Ag compounds at temperatures between 273 and 573 K.

Temp K	273	298	323	373	473	573
Metal cluster						
Ag(0)	0.399	0.335	0.285	0.214	0.133	0.091
Hydroxides						
$Ag(H_2O)_2^+$	0.778	0.659	0.565	0.428	0.269	0.185
$Ag(H_2O)_4^+$	0.556	0.469	0.401	0.303	0.190	0.130
$Ag(H_2O)_6^+$	0.424	0.358	0.307	0.233	0.145	0.099
$AgOH(H_2O)^0$	1.203	1.024	0.882	0.673	0.427	0.294
Carbonates						
$AgHCO_3(H_2O)^0$	0.989	0.838	0.719	0.545	0.343	0.236
$AgHCO_3(OH)^-$	1.384	1.176	1.011	0.769	0.487	0.335
$Ag_2CO_3(H_2O)_2^0$	0.980	0.830	0.712	0.539	0.340	0.233
Chloride compounds						
$AgCl(H_2O)^0$	0.945	0.800	0.685	0.518	0.326	0.223
$AgCl(H_2O)_3^0$	0.933	0.789	0.676	0.512	0.322	0.220
$AgCl(H_2O)_5^0$	0.991	0.838	0.718	0.544	0.342	0.234
$AgCl_2^-$	0.852	0.720	0.616	0.465	0.292	0.200
$AgCl_3^{2-}$	0.308	0.259	0.220	0.165	0.103	0.070
$NaAgCl_2(H_2O)_8$	0.711	0.600	0.513	0.387	0.242	0.166
Sulfide compounds						
$AgSO_4(H_2O)^-$	0.676	0.571	0.489	0.370	0.233	0.160
$AgHSO_4(H_2O)^0$	0.932	0.789	0.677	0.513	0.323	0.221
$Ag_2SO_4(H_2O)_2^0$	0.936	0.792	0.679	0.514	0.324	0.222
$AgHS(H_2O)^0$	0.905	0.765	0.656	0.496	0.312	0.214
$Ag_2HS(H_2O)_2^+$	0.838	0.708	0.606	0.459	0.288	0.197
$Ag_2S(H_2O)_2^0$	0.864	0.731	0.625	0.473	0.297	0.203
$AgSb_2S_6(H_2O)_5^-$	0.505	0.425	0.363	0.273	0.170	0.116
$AgSb_2S_6(H_2O)_6^-$	0.563	0.475	0.406	0.306	0.191	0.131
$AgAs_2S_6(H_2O)_6^-$	0.622	0.525	0.449	0.338	0.212	0.145
Ammonium compounds						
$AgNH_3(H_2O)^+$	0.957	0.812	0.698	0.530	0.335	0.230
$Ag(NH_3)_2^+$	1.131	0.961	0.826	0.629	0.398	0.274

Table 2
Ag—X bond length (X = OH, O_2, OCO_2, Cl, S, OSO_3, N) and 1000 ln β values for the different Ag species considered in this work.

Species	Formula	Bond type	Bond length (Å)[a]	1000 ln β (298 K)
Hydrated Ag^+	$Ag(H_2O)_2^+$	Ag—OH_2	2.182	0.659
	$Ag(H_2O)_4^+$	Ag—OH_2	2.278	0.469
	$Ag(H_2O)_6^+$	Ag—OH_2	2.548	0.358
Hydroxide	$Ag(OH)(H_2O)^0$	Ag—OH	1.999	1.024
	$Ag(OH)HCO_3^-$	Ag—OH	2.030	1.176
Carbonates	$AgHCO_3(H_2O)^0$	Ag—OCO_2	2.106	0.838
	$Ag_2CO_3(H_2O)_2^0$	Ag—OCO_2	2.116	0.830
Chlorides	$AgCl(H_2O)^0$	Ag—Cl	2.300	0.800
	$AgCl(H_2O)_3^0$	Ag—Cl	2.333	0.789
	$AgCl(H_2O)_5^0$	Ag—Cl	2.327	0.838
	$AgCl_2^-$	Ag—Cl	2.374	0.720
	$AgCl_3^{2-}$	Ag—Cl	2.645	0.259
	$NaAgCl_2(H_2O)_8$	Ag—Cl	2.434	0.600
Sulfides	$AgHS(H_2O)^0$	Ag—S	2.327	0.765
	$Ag_2HS(H_2O)_2^+$	Ag—S	2.381	0.708
	$Ag_2S(H_2O)_2^0$	Ag—S	2.312	0.731
Sulfates	$AgSO_4(H_2O)^-$	Ag—OSO_3	2.154	0.571
	$AgHSO_4(H_2O)^0$	Ag—OSO_3	2.117	0.789
	$Ag_2SO_4(H_2O)_2^0$	Ag—OSO_3	2.130	0.792
Sulfo-antimonides	$AgSb_2S_6(H_2O)_6^-$	Ag—S	2.493	0.475
	$AgSb_2S_6(H_2O)_5^-$	Ag—S	2.573	0.425
Sulfo-arsenides	$AgAs_2S_6(H_2O)_6^-$	Ag—S	2.467	0.525
Ammines	$AgNH_3(H_2O)^+$	Ag—N	2.153	0.812
	$Ag(NH_3)_2^+$	Ag—N	2.152	0.961

[a] Nearest neighbor.

hydroxide, complexation of Ag^+ with Cl^- may be a key of the isotope fractionation of Ag.

We further investigated ln β of Ag chlorides. The higher order complexation of Ag^+ with Cl^- forms $AgCl_2^-$. Though a threefold complexation of $AgCl_2(H_2O)^-$ was reported in an MD study (Liu et al., 2012), in our DFT study, the calculation was converged to be a simple linear $AgCl_2^-$. This complex showed smaller ln β compared with that of $AgCl(H_2O)$. In an S free high-temperature/high-pressure fluid, $NaAgCl_2$ is thought to be a dominant Ag species (Yin and Zajacz, 2017). $NaAgCl_2$ may form via the association of hydrated Na^+ and $AgCl_2^-$. A complexation of Na^+ and $AgCl_2^-$ with 8 water molecules was computed. As shown in Table 2, $NaAgCl_2(H_2O)_8$ showed smaller ln β compared with that of $AgCl_2^-$. The magnitude of ln β for the Ag chlorides was on the order of $AgCl(H_2O) > AgCl_2^- > NaAgCl_2(H_2O)_8$.

The nuclear field shift (NFS) effect (see Schauble (2007) and Fujii et al. (2009a) and references therein) was implemented in the DIRAC 13 (Visscher, 2013) program. The triple-zeta Dyall basis sets dyall.cv3z (Dyall, 2007) were used for the relativistic calculation of molecular electronic structures. The electronic structures of Ag^0 and Ag^+ were calculated as those of ($[Kr]4d^{10}5s^1$) and ($[Kr]4d^{10}$), respectively. The NFS effect was only estimated for ^{109}Ag-^{107}Ag fractionation between Ag metal and dissolved sulfide $AgSH(H_2O)$.

3. RESULTS

The structures obtained upon convergence are shown in Fig. 2. The ln β values are tabulated in Table 1 and displayed in Fig. 3 for temperatures of 298 K (25 °C) and 300 °C. Bond lengths are listed in Table 2. In general, chlorides, sulfates, and sulfide with coordination numbers of 1 or 2 fractionate Ag isotopes to the same extent. As expected, compounds with large coordination numbers such as $Ag(H_2O)_6^+$ and $AgCl_3^{2-}$ tend to have smaller ln β values than those with small coordination numbers and close to those of metallic Ag. The larger the number of H_2O or Cl^- around Ag^+, the smaller the ln β. The value of ln β correlates negatively with bond length in two distinct groups (Fig. 4). The largest of these groups consists of Ag^+ hexahydrate, chlorides, sulfides, sulfo-antimonides, and sulfo-arsenides, while the smaller group consists of Ag^+ di- and tetra-hydrate, Ag(OH) mono-hydrate, and hydrated sulfates. As a rule, N and O donor ligand systems show shorter bond lengths and larger ln β values. Sulfur donor ligand systems show longer bond lengths and smaller ln β values. Although the bond lengths of Cl systems are similar to those of the group of S donor systems, their ln β falls in between the values of the O-N group and those of the S group. This trend is similar to those observed for the isotopes of Fe, Ni, Cu, and Zn (Fujii et al., 2014) and seems to correlate negatively with the electronegativity of the bonding ion from O (3.44), N (3.04), Cl (3.16), and S (2.58) (Allred, 1961) and positively with the group electronegativity (Huheey, 1965) (see Table 7 in Fujii et al. (2014)).

To the best of our knowledge, for hydrated Ag^+ ion in aqueous solutions, the molecular vibration between Ag and O of water molecules has not been clarified by IR and Raman spectrometry. According to a study of H_2O adsorption on Ag surface (Stuve et al., 1981), it is suggested

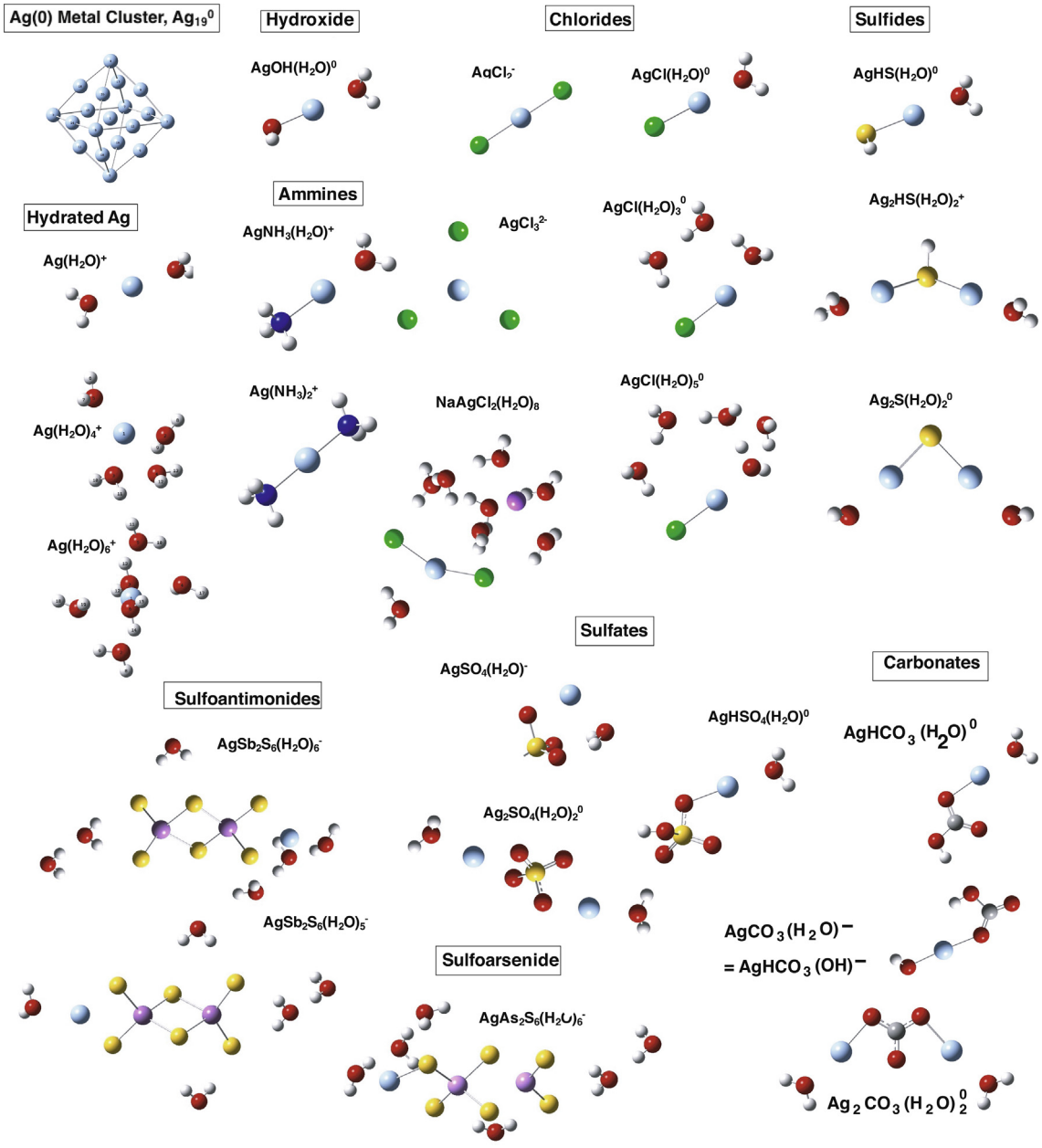

Fig. 2. Structures of some Ag compounds obtained by DFT after convergence.

that Ag—OH_2 stretching frequency may be 200–300 cm^{-1}. Besides the hydrated Ag^+ ion, there are several reports on the vibrational frequencies of Ag(I) complexes. These are shown in Table 3. Our computational results are in good agreement with the literature values.

For the Ag(0)-Ag(I) equilibrium, the NFS effect becomes prominent ($>1 \times 10^{-4}$) at ambient temperature and below (Table 4), but is still on the order of 0.5 epsilon units at 300–500 °C.

4. DISCUSSION

At 25 °C, Ag speciation is critically dependent on Cl concentrations (Fritz, 1985). At the high temperatures of hydrothermal solutions (~300 °C), and in the absence of Sb and As, the predominant species in fluids are $AgCl_2^-$ and $AgHS^0$ (Akinfiev and Zotov, 2001). It must be noted that the speciation adopted by the authors and reproduced in Fig. 5 does not exactly match the species listed in Table 1. The $^{109}Ag/^{107}Ag$ fractionation of these two species is on the order of 10^{-4} at most. Hydroxide AgOH should be found only in S- and Cl-poor fluids and, therefore, can be neglected. Assuming that solid Ag_2S precipitates from the isochemical dissolved species, isotope fractionation between solid Ag_2S and the dissolved $Ag_2S(H_2O)_2^0$ species should be small; not much isotopic fractionation (0.05 epsilon units) is expected in the Ag-Cl-S system regardless of the pH.

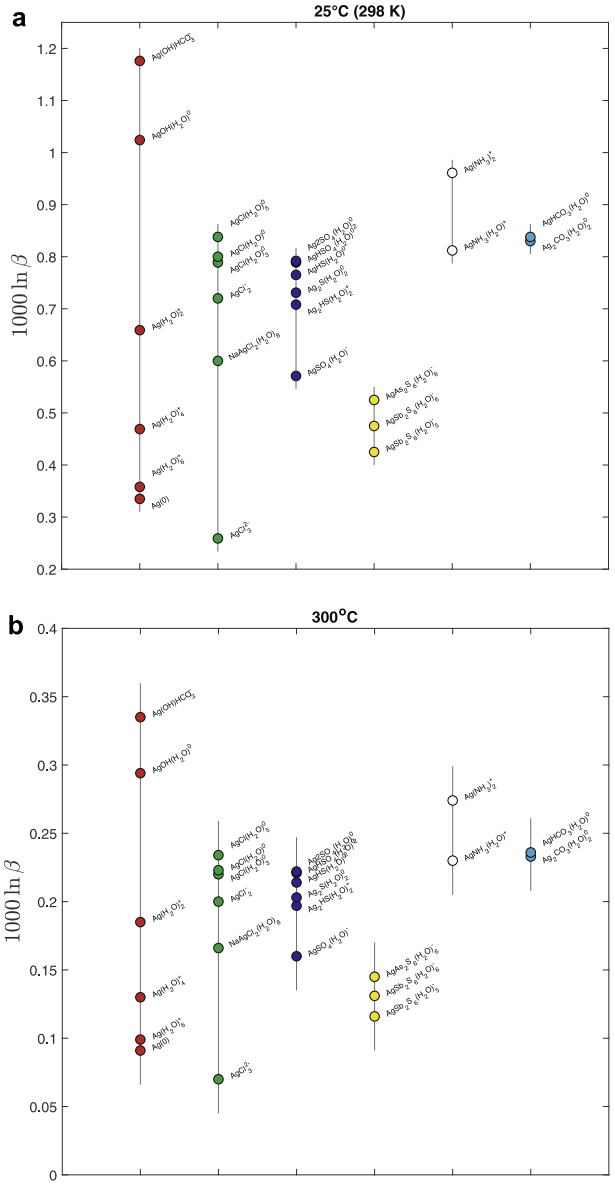

Fig. 3. Ratios of reduced partition functions, in the form 1000 ln β are compared for the isotopomers of Ag^+, Ag hydroxides (red), chlorides (green), sulfides (blue) and sulfates (cyan), Sb- and As-sulfides (yellow), and ammines (white) at temperatures of (a) 298 K (25 °C), relevant to low-temperature processes and analytical protocols, and (b) 573 K (300 °C), relevant to hypogenetic ore genesis. The values for different coordination numbers and hydration shells are compared. (For interpretation of the references to colour in this figure legend, the reader is referred to the web version of this article.)

At those temperatures, stronger effects are, however, expected in Sb- and As-rich solutions. Bonding with SbS_3 clearly reduces the 1000 ln β value by $\sim 2 \times 10^{-4}$ (two epsilon units). Low $^{109}Ag/^{107}Ag$ values are expected in tennantite-tetrahedrite units ($Ag(Sb,As)S_2$) free or substituted in galena, and also in tennantite-tetrahedrite ($Ag(Sb,As)S_3$) precipitated from S-, Cl-, and Pb-rich hydrothermal fluids. Isostructural Sb sulfosalts seem to be isotopically lighter than their As counterparts.

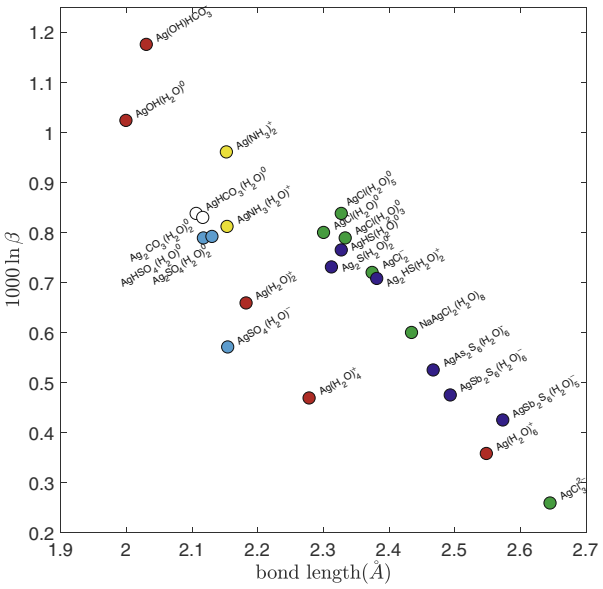

Fig. 4. Correlation between the reduced partition function ratios β of various species at 25 °C and the bond length of Ag to its closest neighbor for different binding groups (legend). The different groups are distributed according to O, N, Cl, and S decreasing electronegativity and increasing group electronegativities (Fujii et al., 2014).

Under the more oxic conditions of the subsurface and at the temperatures of groundwater (<100 °C), silicates are less soluble, alkalinity is lower, Cl is less preponderant, and S should be in the sulfate form. Silver should be present as Ag^+ and, at higher chlorinity, as $AgCl^0$ (Akinfiev and Zotov, 2001). At 100 °C, the $^{109}Ag/^{107}Ag$ ratio should be 2.85×10^{-4} higher for $AgCl^0$ than for Ag^+, which, as an aside to be discussed further below, immediately raises serious concerns when the yield of Ag during separation chemistry is not complete (i.e., less than 100%). It is expected from the results that insoluble chloragyrite (AgCl) should be isotopically heavy.

In groundwater and soils underneath forests and grasslands, ammonia (NH_4^+) should be abundant as a result of nitrogen fixation by diazotrophs, either symbiotically with plants (*rhizobia*) or free-living (*clostridium*), which all work with a family of MoFe or Fe enzymes known as nitrogenases (Bothe et al., 2006). Such enzymes are also particularly abundant in lateritic soils. Silver complexation with NH_4^+ produces a particularly strong complex known as di-ammine silver $Ag(NH_3)_2^+$ (Tollen's reagent). Upon reduction by a number of organic components associated with plants, most commonly aldehydes and catechol melanin, the Tollen's reagent precipitates metallic silver according to the reaction:

$$2Ag(NH_3)_2{}^+(aq) + R\text{-}CHO(aq) + H_2O \rightarrow 2Ag(s) + R\text{-}COOH(aq) + 4NH_3 + 2H^+ \quad (4)$$

Nitrification, e.g., biological oxidation of NH_3 to NO_2^- and NO_3^-, is expected to also destroy di-ammine Ag and precipitate metallic Ag (together with Au and Cu). Metallic Ag nanoparticles (AgNP) are known to precipitate Ag(0) from $AgNO_3$ solutions through the action of bacteria

Table 3
Vibrational frequencies of Ag(I) species.

Species	Stretch	Vibrational frequency (cm^{-1})		References
		This study	Literature	
$Ag(H_2O)_2^+$	Ag—O	285 (ν_1)	200–300	Stuve et al. (1981)
$Ag(H_2O)_4^+$		236 (ν_1)		
$Ag(H_2O)_6^+$		222 (ν_1)		
$AgOH(H_2O)$	O—Ag—O	281 (Ag—OH_2)	280,554	Stuve et al. (1981)lm
		524 (Ag—OH)		Bao et al. (1995)
$AgCl(H_2O)$	O—Ag—Cl	261	227,240	Regis and Corset (1980)
				Fleischmann et al. (1981)
$AgCl_2^-$	Cl—Ag—Cl	247 (ν_1)	238,268 (ν_1)	Waters and Basak (1971)
		84 (ν_2)	88 (ν_2)	Fleischmann et al. (1981)
		314 (ν_3)	290,333 (ν_3)	
$AgHSO_4(H_2O)$	O—Ag—O	241	230	Sasaki and Nishina (1991)
$AgNH_3(H_2O)^+$	O—Ag—N	308	296	Lundeen and Tobias (1975)
$Ag(NH_3)_2^+$	N—Ag—N	350 (ν_1)	329,369 (ν_1)	Miles et al. (1968)
		423 (ν_3)	430 (ν_3)	Lundeen and Tobias (1975)

Table 4
Nuclear Field Shift (NFS) vs mass-dependent (MS) isotope effect for the reduction reaction Ag(I) -> Ag(0) for ^{109}Ag-^{107}Ag fractionation between Ag metal and dissolved sulfide AgSH (H_2O). Values of 1000 ln $\beta_{Ag(0)}$ -1000 ln $\beta_{Ag(I)}$ broken down into MS and NFS effects.

Temp (°C)	MS	NFS	MS + NFS
0	−0.5059	0.1025	−0.4034
25	−0.4304	0.0939	−0.3365
50	−0.3703	0.0866	−0.2837
100	−0.2821	0.0750	−0.2071
200	−0.1786	0.0592	−0.1195
300	−0.1229	0.0488	−0.0741
500	−0.0682	0.0362	−0.0320
700	−0.0432	0.0288	−0.0145
900	−0.0298	0.0239	−0.0060
1100	−0.0279	0.0204	−0.0075

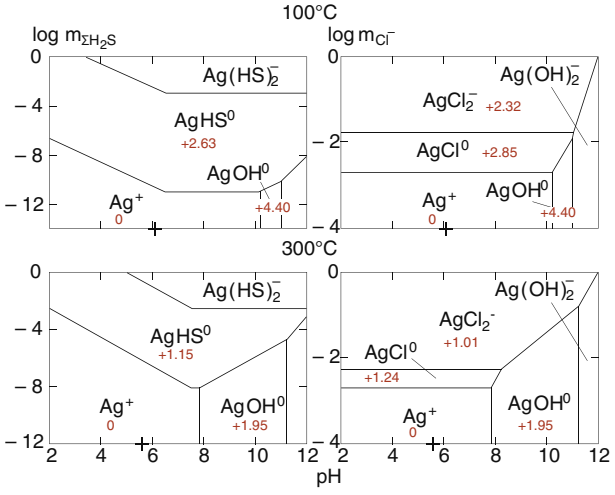

Fig. 5. Stability fields of Ag compounds at 100 and 300 °C and pressures of 1–2000 bars in the Ag-Cl-S-H_2O system (Akinfiev and Zotov, 2001). Numbers in red are $^{109}Ag/^{107}Ag$ fractionation of Ag species relative to Ag^+ in epsilon units.

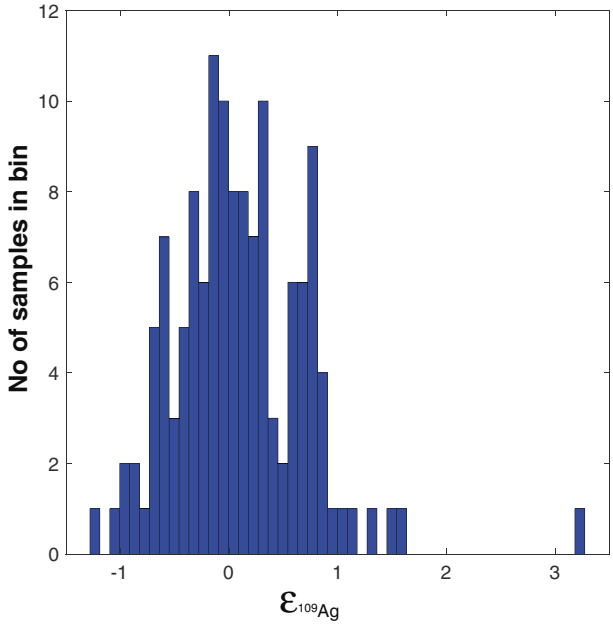

Fig. 6. Histogram of ε_{109Ag} in the 132 silver coins analyzed by Desaulty and Albarede (2013), Desaulty et al. (2011) and Albarède et al. (2016). Typical analytical errors are <0.1 ε units. Note that most values cluster around 0 and are consistent with hydrothermal ores, while a secondary peak at ~+0.8 may signal low-temperature ores (gossan), including native silver biologically formed by the breakdown of diammine Ag.

(*Lactobacillus*, *Pseudomonas*, yeast (MKY3) and fungi (Mandal et al., 2006; Sharma et al., 2009). A silver-resistant strain of *Pseudomonas stutzeri* isolated by Haefeli et al. (1984) from the soils of a silver mine, intracellularly accumulate AgNPs (Slawson et al., 1992). Native Ag, pure or alloyed with Au, is found in soils, in particular in the weathering products of sulfide seams (gossan). If Ag is distributed among Ag^+, $Ag(H_2O)_6^+$, $AgCl_2^-$, and $Ag(NH_3)_2^+$, precipitation of native Ag from di-ammine Ag should favor $^{109}Ag/^{107}Ag$ ratios higher by up to 10 epsilon

Table 5
Parametric and non-parametric tests for the ε_{109Ag} values of the silver coins analyzed by Desaulty and Albarede (2013), Desaulty et al. (2011) and Albarède et al. (2016) grouped by period and provenance and shown in Fig. 1. The matrices of *p*-values (top) and Mann-Whitney-Wilcoxon rank sum test (bottom) allow two different samples to be tested against the hypothesis that they were produced in a single region. Small values, typically 0.00–0.10 (in red) suggest that the groups of coins used metal from different provenances. For example, Medieval and Modern Spain ($p = 0.00$, $U = 0.01$) minted silver coins from unrelated ores. Similar provenances are allowed by the largest values, typically >0.70 (in green).

t-test	*Aver.*		*Std*	*Anc East Mediterr*	*Anc West Mediterr*	*Medieval Europe*	*Medieval Spain*	*Modern Spain*	*Modern Europe*	*Peru*	*Mexico*
Anc East Mediterr	-0.10	±	0.25	1	0.23	0.83	0.52	0.00	0.01	0.06	0.00
Anc. West Mediterr	-0.25	±	0.48	0.23	1	0.34	0.12	0.00	0.00	0.01	0.00
Medieval Europe	-0.07	±	0.48	0.83	0.34	1	0.80	0.01	0.15	0.23	0.00
Medieval Spain	-0.02	±	0.46	0.52	0.12	**0.80**	1	0.00	0.22	0.14	0.00
Modern Spain	0.45	±	0.48	0.00	0.00	0.01	0.00	1	0.02	0.79	0.20
Modern Europe	0.15	±	0.25	0.01	0.00	0.15	0.22	0.02	1	0.24	0.00
Peru	0.54	±	1.32	0.06	0.01	0.23	0.14	**0.79**	0.24	1	0.76
Mexico	0.68	±	0.12	0.00	0.00	0.00	0.00	0.20	0.00	**0.76**	1

Mann-Whitney *U*-test		*Anc East Mediterr*	*Anc West Mediterr*	*Medieval Europe*	*Medieval Spain*	*Modern Spain*	*Modern Europe*	*Peru*	*Mexico*
Anc East Mediterr		1	0.17	1.00	0.72	0.00	0.01	0.24	0.00
Anc. West Mediterr		0.17	1	0.37	0.11	0.00	0.00	0.08	0.00
Medieval Europe		**1.00**	0.37	1	0.72	0.01	0.17	0.31	0.00
Medieval Spain		**0.72**	0.11	**0.72**	1	0.01	0.06	0.25	0.00
Modern Spain		0.00	0.00	0.01	0.01	1	0.00	0.97	0.50
Modern Europe		0.01	0.00	0.17	0.06	0.00	1	0.38	0.00
Peru		0.24	0.08	0.31	0.25	**0.97**	0.38	1	0.89
Mexico		0.00	0.00	0.00	0.00	0.50	0.00	**0.89**	1

units. Variable $^{109}Ag/^{107}Ag$ values have been observed in native Ag and in Ag dissolved in native Au by Chugaev and Chernyshev (2009) and Mathur et al. (2018), which suggests that native metals may indeed form in soils by the action of nitrogen fixation and nitrification. Precipitation of high-$^{109}Ag/^{107}Ag$ metal should leave Ag chelates, notably chlorides, in the residual fluid extremely depleted in ^{109}Ag. At low-temperature, the nuclear field-shift effect associated with redox processes may contribute up to 1 epsilon unit to the scatter of $^{109}Ag/^{107}Ag$, and probably more if finite-reservoir (Rayleigh distillation) conditions prevail.

Planetary reservoir silver contents as compiled by Palme and O'Neill (2003) are 197 ppb in CI chondrites, 4 ppb in the terrestrial mantle, and 80 ppb in average continental crust. We propose that silver coins offer the best representative mean value of $^{109}Ag/^{107}Ag$ in the continental crust simply because of their quite narrow isotopic range in spite of the metal having been mined for 2000 years from ores distributed throughout unrelated orogens spreading over more than thousands of kilometers. The most obvious cause of Ag isotopic variability observed in Fig. 1 is the relative proportions of hydrothermal (galena, sulfosalts) and low-temperature ores (epigenetic, gossan). A histogram of ε_{109Ag} in all silver coins measured so far (Fig. 6) shows a well-defined peak at 0 (relative to NIST SRM 978a) and a smaller peak at +0.8. The statistical distances between the groups of data from different provinces (Peru, Mexico, Europe, E. Mediterranean, etc.) and different periods (Antiquity, Middle Age, Modern, etc) are a useful guideline. Table 5 shows the mean and standard deviation for each province, the matrix of binary parametric (Student's) t-tests, and the matrix of binary non-parametric (Mann-Whitney-Wilcoxon rank sum) tests. The elements of the matrix measure the probability *p* that two groups (row/column) are samples from two normal (Student) or non-necessarily normal (Mann-Whitney-Wilcoxon) populations with the same mean. Large *p* values (>0.7) raise the possibility that silver coins from Medieval Europe, Medieval Spain, and the Antique Eastern Mediterranean shared common Ag sources and therefore that the same ore deposits were mined. This is also the case for coins struck in Peru and for coins struck in Modern (post-Columbus) Spain and in Mexico. Coins from Modern Spain and Mexico are statistically more distant. Additional tracers such as Cu and Pb isotope compositions can help refine the assignment of a particular mint to a particular source (Desaulty et al., 2011; Desaulty and Albarede, 2013).

In contrast, Modern and Medieval Spain are statistically different ($p = 0.00$), which has been ascribed by Desaulty et al. (2011) and Albarede et al. (2012) to two different events. (1) With the conquest of the Granada Emirate in 1492, the silver mines of the Betics, Southern Spain, fell into the hands of the Catholic Kings. (2) After the second half of

the 16th century, Peru and Mexico became the nearly exclusive silver providers of the Spanish crown. The silver mines of Potosi, Peru, and Zacatecas, Mexico, produced enormous amounts of silver, thanks in part to the 'patio' amalgamation process invented by "Bartolomé de Medina" (Probert, 1969; Brading and Cross, 1972). Although the temperatures in excess of 960 °C required by the much older cupellation process are not expected to produce observable isotope fractionation, it is not clear whether an incomplete 'patio' amalgamation process could have introduced some isotopic bias. The narrow range of ε_{109Ag} in silver coins, however, strongly suggests that metallurgy was not the main cause of isotope fractionation.

5. IMPLICATIONS FOR ^{107}PD-^{107}AG CHRONOMETRY AND THE ^{109}AG/^{107}AG OF THE BULK SILICATE EARTH

An important cosmochemical implication of the present work is related to the extinct ^{107}Pd-^{107}Ag chronometer ($T_{1/2} = 6.5$ Ma), which produces positive deviations of a few ε_{109Ag} units in chondrites. Isotopic variability induced by the low-temperature alteration well known to have affected most meteorites, in particular chondrites, has been noted by Woodland et al. (2005), Schönbächler et al. (2008, 2010), and Theis et al. (2013). Note that ^{107}Ag being the radiogenic isotope, cosmochemists use ε_{107Ag} ($=-\varepsilon_{109Ag}$) while we here uphold the stable isotope convention of using heavy/light ratios. The ε_{107Ag} values of the carbonaceous chondrites analyzed by Schönbächler et al. (2008) (-2.1 to $+0.8$) are similar to the Bulk Silicate Earth (BSE) (-2.2 ± 0.7) proposed by Schönbächler et al. (2010). The validity of this BSE value, which was derived from a set of basalt data with Ag chemistry yields as low as 60 percent, is questionable. The difference of 0.9 ε_{107Ag} units between two series of measurements of Allende (CV3 chondrite) and the difference of 15 ε_{107Ag} units between two series of measurements of the same Hawaiian lava sample KOO49 analyzed by Schönbächler et al. (2008) and Theis et al. (2013) are significantly larger than the reproducibility of the measurements. Although the authors attribute these differences to sample heterogeneity, the present work suggests that incomplete Ag yields during anion-exchange separation in chloride-bearing media (Schönbachler et al., 2007) may also be the cause of the observed analytical biases.

In contrast, the average ε_{107Ag} in the metal of 132 silver coins, which together represent a massive amount of geographically widespread terrestrial metal minted over 2000 years and dominated by hydrothermal deposits, is -0.10 ± 0.10 (2-sigma standard error). This value is strikingly similar to the NIST SRM 978a value ($\varepsilon_{107Ag} = \varepsilon_{109Ag} \equiv 0$), especially if the gossan-type, ^{109}Ag-rich silver component of the second peak on the histogram of Fig. 6 is taken into account. This value also is similar to Theis et al.'s (2013) data on a Coddy Shale sample. Although reliable isotopic data on terrestrial rocks and ores are scarce, petrological evidence suggests that Ag is quantitatively transferred to the liquid phase during mantle melting, and that Ag is quantitatively partitioned into sulfide melt during magma ascent and cooling (Li and Audétat, 2012; Kiseeva and Wood, 2015). With all these processes taking place at high temperatures, which is consistent with the remarkably narrow ε_{109Ag} range of silver coinage, it is expected that Ag isotope fractionation between the crust and the mantle is minor. We therefore suggest that the NIST SRM 978a value should be retained to represent the Bulk Silicate Earth. Since addition of chondritic material should have little or no impact on the ^{109}Ag/^{107}Ag of a chondritic Earth, the more radiogenic character of Ag in the BSE relative to chondrites is consistent with the accretion of a small veneer of iron meteorites, which may be a component of the Late Veneer recognized by Chou (1978).

In contrast, and as suggested by Schönbächler et al. (2008), the pronounced scatter of ordinary chondrite data, however, most likely reflects open system metamorphism on the parent body. The fractionation factors at ambient temperatures derived from the present study are of a magnitude consistent with such a difference.

6. CONCLUSIONS

We calculated by DFT the ratios of ^{109}Ag/^{107}Ag reduced partition function ratios ln β for the free Ag^+ ion with various degrees of hydration, for hydrates, chloride complexes, sulfides, sulfates, Sb-As sulfosalts, carbonates, and Ag-ammines. At 0 °C, the magnitude of the Nuclear Field Shift effect on isotope ratios is -1×10^{-4}. Only weak Ag isotope fractionation is expected at 300 °C in the Ag-Cl-S system regardless of the pH of hydrothermal solutions. Bonding with SbS_3 and AsS_3 reduces ln β values in a temperature-dependent way.

At low temperatures, chlorides and native silver should be fractionated relative to the hydrated Ag^+ ion. In groundwater underneath forests and grasslands, Ag^+ forms diammine silver with ammonia resulting from nitrogen fixation and, upon biologically-mediated reduction, precipitates metallic Ag(0).

It is suggested that incomplete Ag yields during anion-exchange separation is an issue that may have affected published ^{109}Ag/^{107}Ag data on chondrites and terrestrial silicate rocks.

Analytical issues raise some questions about the reliability of literature values on silicate rocks and meteorites: we propose that the NIST SRM 978a value ($\varepsilon_{107Ag} = \varepsilon_{109Ag} \equiv 0$) should be adopted as the new BSE reference.

ACKNOWLEDGMENTS

We acknowledge support from the European Research Council grant 741454-SILVER-ERC-2016-ADG. TF thanks Minori Abe for her valuable comments on the NFS calculation. Janne Blichert-Toft did a great job editing the English and polishing the text. We gratefully acknowledge insightful comments by three anonymous referees.

APPENDIX

Mineralogy of some ore deposits of historical importance (Boyle, 1968).

Potosi (quartz-porphyry), Peru: Ag sulfides and sulfosalts: tetrahedrite $Cu_{12}([As,Sb]S_3)_4S$, andorite ($PbAgSb_3S_6$), pyrargyrite (Ag_3SbS_3), matildite ($AgBiS_2$). Oxidation to >300 m: native silver, chlorargyrite, Ag_2S, pyrargyrite.

Zacatecas (stockwork in sediments), Mexico: tetrahedite, argentiferous galena, argentite, pyragyrite. Secondary minerals: native silver, argentite, chlorargyrite.

Laurion (replacement of carbonates and calcareous schists), Greece: The chief high-temperature Ag ore is argentiferous galena. The deeply oxidized deposits are very rich in silver with occurrence of native silver.

Jáchymov (Joachimsthal), Czech Republic: silver is present in various sulfosalts and argentite.

REFERENCES

Akinfiev N. and Zotov A. (2001) Thermodynamic description of chloride, hydrosulfide, and hydroxo complexes of Ag (I), Cu (I), and Au (I) at temperatures of 25–500°C and pressures of 1–2000 bar. *Geochem. Int.* **39**, 990–1006.

Albarède F., Blichert-Toft J., Rivoal M. and Telouk P. (2016) A glimpse into the Roman finances of the Second Punic War through silver isotopes. *Geochem. Perspect. Lett.* **2**, 127–137.

Albarede F., Desaulty A. M. and Blichert-Toft J. (2012) A geological perspective on the use of Pb isotopes in archeometry. *Archaeometry* **54**, 853–867.

Allred A. (1961) Electronegativity values from thermochemical data. *J. Inorg. Nucl. Chem.* **17**, 215–221.

Baes C. J. and Mesmer R. (1976) *The Hydrolysis of Cations*. John Wiley and Sons, New York.

Baker, H. and Okamoto, H. (1992) ASM Handbook: Volume 3: Alloy Phase Diagrams ASM International. Materials Park.

Bao X., Muhler M., Pettinger B., Uchida Y., Lehmpfuhl G., Schlögl R. and Ertl G. (1995) The effect of water on the formation of strongly bound oxygen on silver surfaces. *Catal. Lett.* **32**, 171–183.

Becke A. D. (1993) Density-functional thermochemistry. III. The role of exact exchange. *J. Chem. Phys.* **98**, 5648–5652.

Bigeleisen J. (1996) Nuclear size and shape effects in chemical reactions: Isotope chemistry of the heavy elements. *J. Am. Chem. Soc.* **118**, 3676–3680.

Bigeleisen J. and Mayer M. G. (1947) Calculation of equilibrium constants for isotopic exchange reactions. *J. Chem. Phys.* **15**, 261–267.

Blanchard M., Balan E. and Schauble E. A. (2017) Equilibrium fractionation of non-traditional isotopes: a molecular modeling perspective. *Rev. Mineral. Geochem.* **82**, 27–63.

Blauth C. M., Pribil A. B., Randolf B. R., Rode B. M. and Hofer T. S. (2010) Structure and dynamics of hydrated Ag+: An ab initio quantum mechanical/charge field simulation. *Chem. Phys. Lett.* **500**, 251–255.

Blichert-Toft J., Delile H., Lee C. T., Stos-Gale Z., Billström K., Andersen T., Hannu H. and Albarède F. (2016) Large-scale tectonic cycles in Europe revealed by distinct Pb isotope provinces. *Geochem., Geophys., Geosyst.* **17**, 3854–3864.

Bothe H., Ferguson S. and Newton W. E. (2006) *Biology of the Nitrogen Cycle*. Elsevier.

Boyle, R.W. (1968) The geochemistry of silver and its deposits: with notes on geochemical prospecting for the element, Bulletin 160. Geological Survey of Canada.

Brading D. A. and Cross H. E. (1972) Colonial silver mining: Mexico and Peru. *Hispanic Am. Hist. Rev.* **52**, 545–579.

Breit G. (1958) Theory of isotope shift. *Rev. Mod. Phys.* **30**, 507–516.

Brill R. H. and Shields W. R. (1972) Lead isotopes in ancient coins, Methods of chemical and metallurgical investigation of ancient coinage: a symposium held by the Royal Numismatic Society in London on 9–11 December 1970. *Roy. Numismatic Soc.*, 279–303.

Brix P. and Kopfermann H. (1958) Isotope shift studies of nuclei. *Rev. Mod. Phys.* **30**, 517–520.

Budd P., Haggerty R., Pollard A., Scalife B. and Thomas R. (1996) Rethinking the quest for provenance. *Antiquity* **70**, 168–174.

Chou C. L. (1978) Fractionation of siderophile elements in the Earth's upper mantle. *Proc. Lunar Planet. Sci. Conf.* **9**, 219–230.

Chugaev A. V. and Chernyshev I. V. (2009) Variations of ^{107}-Ag/^{109}Ag isotope ratio in ore deposits by high-precision MC-ICP-MS. *Geochim. Cosmochim. Acta* **73**, A225.

Chutas N. I., Kress V. C., Ghiorso M. S. and Sack R. O. (2008) A solution model for high-temperature PbS-AgSbS2-AgBiS2 galena. *Am. Mineral.* **93**, 1630–1640.

Dennington R., Keith T. and Millam J. (2009) *GaussView, version 5*. Semichem Inc., Shawnee Mission, KS.

Desaulty A. M. and Albarede F. (2013) Copper, lead, and silver isotopes solve a major economic conundrum of Tudor and early Stuart Europe. *Geology* **41**, 135–138.

Desaulty A. M., Telouk P., Albalat E. and Albarede F. (2011) Isotopic Ag-Cu-Pb record of silver circulation through 16th-18th century Spain. *PNAS* **108**, 9002–9007.

Dyall, K.G. (2007) Relativistic double-zeta, triple-zeta, and quadruple-zeta basis sets for the 4d elements Y–Cd. Theoret. Chem. Acc.: Theory, Comput., Model.ing (Theoretica Chimica Acta) 117, 483–489.

Figgen D., Rauhut G., Dolg M. and Stoll H. (2005) Energy-consistent pseudopotentials for group 11 and 12 atoms: adjustment to multi-configuration Dirac–Hartree–Fock data. *Chem. Phys.* **311**, 227–244.

Fleischmann M., Hendra P., Hill I. and Pemble M. (1981) Enhanced Raman spectra from species formed by the coadsorption of halide ions and water molecules on silver electrodes. *J. Electroanal. Chem. Interfacial Electrochem.* **117**, 243–255.

Flynn D. O. and Giraldez A. (1996) China and the Spanish Empire. *Rev. Hist. Econ.* **14**, 309–338.

Frisch, M., Trucks, G., Schlegel, H., Scuseria, G., Robb, M., Cheeseman, J., Scalmani, G., Barone, V., Mennucci, B. and Petersson, G. (2009) Gaussian 09, revision D. 01. Gaussian, Inc., Wallingford CT.

Fritz J. J. (1985) Thermodynamic properties of chloro-complexes of silver chloride in aqueous solution. *J. Solut. Chem.* **14**, 865–879.

Fujii T., Moynier F. and Albarede F. (2006a) Nuclear field vs. nucleosynthetic effects as cause of isotopic anomalies in the early Solar System. *Earth Planet. Sci. Lett.* **247**, 1–9.

Fujii T., Moynier F. and Albarede F. (2009a) The nuclear field shift effect in chemical exchange reactions. *Chem. Geol.* **267**, 139–156.

Fujii T., Moynier F., Blichert-Toft J. and Albarede A. F. (2014) Density functional theory estimation of isotope fractionation of Fe, Ni, Cu, and Zn among species relevant to geochemical and biological environments. *Geochim. Cosmochim. Acta* **140**, 553–576.

Fujii T., Moynier F., Telouk P. and Abe M. (2010) Experimental and theoretical investigation of isotope fractionation of zinc between aqua, chloro, and macrocyclic complexes. *J. Phys. Chem. A* **114**, 2543–2552.

Fujii T., Moynier F., Telouk P. and Albarede F. (2009b) Nuclear field shift effect in the isotope exchange reaction of cadmium using a crown ether. *Chem. Geol.* **267**, 157–163.

Fujii, T., Moynier, F., Telouk, P. and Albarède, F. (2006b) Mass-independent isotope fractionation of molybdenum and ruthenium and the origin of isotopic anomalies in Murchison. Astroph. J., 647, 1506–1516.

Fulton J. L., Kathmann S. M., Schenter G. K. and Balasubramanian M. (2009) Hydrated structure of Ag (I) ion from symmetry-dependent, K-and L-edge XAFS multiple scattering and molecular dynamics simulations. *J. Phys. Chem. A* **113**, 13976–13984.

Garner R. L. (1988) Long-term silver mining trends in Spanish America: a comparative analysis of Peru and Mexico. *Amer. Hist. Rev.* **XCIII**, 898–935.

Gentner W., Müller O., Wagner G. and Gale N. (1978) Silver sources of archaic Greek coinage. *Naturwissenschaften* **65**, 273–284.

George L., Cook N. J., Cristiana L. and Wade B. P. (2015) Trace and minor elements in galena: A reconnaissance LA-ICP-MS study. *Am. Mineral.* **100**, 548–569.

Ginovska B., Camaioni D. M., Dupuis M., Schwerdtfeger C. A. and Gil Q. (2008) Charge-dependent cavity radii for an accurate dielectric continuum model of solvation with emphasis on ions: aqueous solutes with oxo, hydroxo, amino, methyl, chloro, bromo, and fluoro functionalities. *J. Phys. Chem. A* **112**, 10604–10613.

Haefeli C., Franklin C. and Hardy K. E. (1984) Plasmid-determined silver resistance in Pseudomonas stutzeri isolated from a silver mine. *J. Bacteriol.* **158**, 389–392.

Hauri, E., Carlson, R. and Bauer, J. (2000) The timing of core formation and volatile depletion in solar system objects from high-precision 107Pd-107Ag isotope systematics. In Lunar and Planetary Science Conference, p. 1812.

Hong S., Candelone J.-P., Patterson C. C. and Boutron C. F. (1994) Greenland ice evidence of hemispheric lead pollution two millennia ago by Greek and Roman civilizations. *Science* **265**, 1841–1843.

Huheey J. E. (1965) The electronegativity of groups. *J. Phys. Chem.* **69**, 3284–3291.

King W. H. (1984) *Isotope Shifts in Atomic Spectra*. Plenum, New York.

Kiseeva E. S. and Wood B. J. (2015) The effects of composition and temperature on chalcophile and lithophile element partitioning into magmatic sulphides. *Earth Planet. Sci. Lett.* **424**, 280–294.

Klein S., Brey G. P., Durali-Müller S. and Lahaye Y. (2010) Characterisation of the raw metal sources used for the production of copper and copper-based objects with copper isotopes. *Archaeol. Anthropol. Sci.* **2**, 45–56.

Kylander M. E., Weiss D. J., Cortizas A. M., Spiro B., Garcia-Sanchez R. and Coles B. (2005) Refining the pre-industrial atmospheric Pb isotope evolution curve in Europe using an 8000 year old peat core from NW Spain. *Earth Planet. Sci. Lett.* **240**, 467–485.

L. Visscher, H.J.A.J., R. Bast, and T. Saue, with contributions from V. Bakken, K. G. Dyall, S. Dubillard, U. Ekström, E. Eliav, T. Enevoldsen, E. Faßhauer, T. Fleig, O. Fossgaard, A. S. P. Gomes, T. Helgaker, J. K. Lærdahl, Y. S. Lee, J. Henriksson, M. Iliaš, Ch. R. Jacob, S. Knecht, S. Komorovský, O. Kullie, C. V. Larsen, H. S. Nataraj, P. Norman, G. Olejniczak, J. Olsen, Y. C. Park, J. K. Pedersen, M. Pernpointner, K. Ruud, P. Sałek, B. Schimmelpfennig, J. Sikkema, A. J. Thorvaldsen, J. Thyssen, J. van Stralen, S. Villaume, O. Visser, T. Winther, and S. Yamamoto (see http://www.diracprogram.org) (2013) DIRAC, a relativistic ab initio electronic structure program, Release DIRAC13 (2013).

Lee C., Yang W. and Parr R. G. (1988) Development of the Colle-Salvetti correlation-energy formula into a functional of the electron density. *Phys. Rev. B* **37**, 785.

Li Y. and Audétat A. (2012) Partitioning of V, Mn Co, Ni, Cu, Zn, As, Mo, Ag, Sn, Sb, W, Au, Pb, and Bi between sulfide phases and hydrous basanite melt at upper mantle conditions. *Earth Planet. Sci. Lett.* **355**, 327–340.

Liu X., Lu X., Wang R. and Zhou H. (2012) Silver speciation in chloride-containing hydrothermal solutions from first principles molecular dynamics simulations. *Chem. Geol.* **294**, 103–112.

Lundeen J. and Tobias R. (1975) Evidence for ion pairing and solvation from Raman spectra of solutions of ammonium, silver, potassium, sodium, and calcium nitrates in liquid ammonia. *J. Chem. Phys.* **63**, 924–934.

Maeda M., Maegawa Y., Yamaguchi T. and Ohtaki H. (1979) X-ray diffraction studies on the structures of diammine-and aquasilver (I) complexes in aqueous solution. *Bull. Chem. Soc. Jpn.* **52**, 2545–2550.

Magini, M. (2018) X-ray Diffraction of Ions in Aqueous Solutions: Hydration and Complex Formation. CRC Press.

Mandal D., Bolander M. E., Mukhopadhyay D., Sarkar G. and Mukherjee P. (2006) The use of microorganisms for the formation of metal nanoparticles and their application. *Appl. Microbiol. Biotechnol.* **69**, 485–492.

Mathur R., Arribas A., Megaw P., Wilson M., Stroup S., Meyer-Arrivillaga D. and Arribas I. (2018) Fractionation of silver isotopes in native silver explained by redox reactions. *Geochim. Cosmochim. Acta* **224**, 313–326.

McLaughlin R. (2014) *The Roman Empire and the Indian Ocean: The Ancient World Economy and the Kingdoms of Africa*. Arabia and India, Pen and Sword.

Miles M., Patterson J., Hobbs C., Hopper M., Overend J. and Tobias R. (1968) Raman and infrared spectra of isosteric diammine and dimethyl complexes of heavy metals. Normal-coordinate analysis of (X3Y2) 2Z ions and molecules. *Inorg. Chem.* **7**, 1721–1729.

Palme, H. and O'Neill, H.S.C. (2003) Cosmochemical estimates of mantle composition. In Carlson, R. W. (Ed.), Treatise on Geochemistry, vol. 2. The Mantle and Core. Elsevier, pp. 1–38.

Parker, A. (1992) Ancient Shipwrecks of the Mediterranean and the Roman Provinces (BAR Int. S. 580). Oxford.

Persson I. and Nilsson K. B. (2006) Coordination Chemistry of the Solvated Silver (I) Ion in the Oxygen Donor Solvents Water, Dimethyl Sulfoxide, and N, N′-Dimethylpropyleneurea. *Inorg. Chem.* **45**, 7428–7434.

Peterson, K.A. and Puzzarini, C. (2005) Systematically convergent basis sets for transition metals. II. Pseudopotential-based correlation consistent basis sets for the group 11 (Cu, Ag, Au) and 12 (Zn, Cd, Hg) elements. Theoret. Chem. Acc.: Theory, Comput., Model. (Theoretica Chimica Acta), 114, 283–296.

Probert A. (1969) Bartolomé de Medina: the patio process and the sixteenth century silver crisis. *J. West* **8**, 90–124.

Regis A. and Corset J. (1980) A chemical interpretation of the intense Raman spectra observed at a silver electrode in the presence of chloride ion and pyridine: formation of radicals. *Chem. Phys. Lett.* **70**, 305–310.

Renock D. and Becker U. (2011) A first principles study of coupled substitution in galena. *Ore Geol. Rev.* **42**, 71–83.

Rustad J. R., Casey W. H., Yin Q.-Z., Bylaska E. J., Felmy A. R., Bogatko S. A., Jackson V. E. and Dixon D. A. (2010) Isotopic fractionation of Mg2+(aq), Ca2+(aq), and Fe2+(aq) with carbonate minerals. *Geochim. Cosmochim. Acta* **74**, 6301–6323.

Sandstrom M., Neilson G., Johansson G. and Yamaguchi T. (1985) Ag+ hydration in perchlorate solution. *J. Phys. C: Solid State Phys.* **18**, L1115.

Sasaki Y. and Nishina Y. (1991) Raman study of a silver electrode in electrolytes with SO_4^{2-} ions. *Surf. Sci.* **242**, 549–553.

Schauble E. A. (2007) Role of nuclear volume in driving equilibrium stable isotope fractionation of mercury, thallium, and other very heavy elements. *Geochim. Cosmochim. Acta* **71**, 2170–2189.

Scheidel W. (2009) In search of Roman economic growth. *J. Roman Archaeol.* **22**, 46–70.

Schönbachler M., Carlson R. W., Horan M. F., Mock T. D. and Hauri E. H. (2007) High precision Ag isotope measurements in geologic materials by multiple-collector ICPMS: An evaluation of dry versus wet plasma. *Int. J. Mass Spectrom.* **261**, 183–191.

Schönbächler M., Carlson R. W., Horan M. F., Mock T. D. and Hauri E. H. (2008) Silver isotope variations in chondrites: volatile depletion and the initial 107Pd abundance of the solar system. *Geochim. Cosmochim. Acta* **72**, 5330–5341.

Schönbächler M., Carlson R. W., Horan M. F., Mock T. D. and Hauri E. H. (2010) Heterogeneous accretion and the moderately volatile element budget of Earth. *Science* **328**, 884–887.

Sharma V. K., Yngard R. A. and Lin Y. (2009) Silver nanoparticles: green synthesis and their antimicrobial activities. *Adv. Colloid Interface Sci.* **145**, 83–96.

Slawson R. M., Van Dyke M. I., Lee H. and Trevors J. T. (1992) Germanium and silver resistance, accumulation, and toxicity in microorganisms. *Plasmid* **27**, 72–79.

Spate, O. H. K. (2013) The Spanish Lake. ANU Press.

Stos-Gale Z. A. and Gale N. H. (2009) Metal provenancing using isotopes and the Oxford archaeological lead isotope database (OXALID). *Archaeol. Anthropol. Sci.* **1**, 195–213.

Stuve E., Madix R. and Sexton B. (1981) The adsorption and reaction of H2O on clean and oxygen covered Ag (110). *Surf. Sci.* **111**, 11–25.

Theis K., Schönbächler M., Benedix G., Rehkämper M., Andreasen R. and Davies C. (2013) Palladium–silver chronology of IAB iron meteorites. *Earth Planet. Sci. Lett.* **361**, 402–411.

Tomasi J., Mennucci B. and Cammi R. (2005) Quantum mechanical continuum solvation models. *Chem. Rev.* **105**, 2999–3094.

Urey H. C. (1947) The thermodynamic properties of isotopic substances. *J. Chem. Soc. (London)*, 562–581.

Van Hook H. J. (1960) The ternary system Ag_2S-Bi_2S_3-PbS. *Econ. Geol.* **55**, 759–788.

von Glahn R. (2003) Money use in China and changing patterns of global trade in monetary metals, 1500–1800. In *Global Connections and Monetary History, 1470–1800* (eds. D. O. Flynn, A. Giraldez and R. von Glahn). Ashgate, Burlington, pp. 187–205.

Waters, D. and Basak, B. (1971) Vibrational spectra of dihalogenoanions of copper (I) and silver (I) in solution in tri-n-butyl phosphate. J. Chem. Soc. A: Inorg., Phys., Theoret., 2733–2735.

Woodland S. J., Rehkamper M., Halliday A. N., Lee D. C., Hattendorf B. and Gunther D. (2005) Accurate measurement of silver isotopic compositions in geological materials including low Pd/Ag meteorites. *Geochim. Cosmochim. Acta* **69**, 2153–2163.

Yin, Y. and Zajacz, Z. (2017) The solubility of sliver in magmatic fluids. In Goldschmidt Conference, Paris, 4409.

Associate editor: Shichun Huang